Accepted Manuscript

Strengthening of RC beams using bottom and side NSM reinforcement

Cristian Sabau, Cosmin Popescu, Gabriel Sas, Jacob W. Schmidt, Thomas Blanksvärd, Björn Täljsten

PII: S1359-8368(18)30587-0

DOI: 10.1016/j.compositesb.2018.05.011

Reference: JCOMB 5681

To appear in: *Composites Part B*

Received Date: 22 February 2018

Revised Date: 24 April 2018

Accepted Date: 9 May 2018

Strengthening of RC beams using bottom and side NSM reinforcement

Cristian Sabau[a],*; Cosmin Popescu[b]; Gabriel Sas[a]; Jacob W. Schmidt[c]; Thomas Blanksvärd[a] and Björn Täljsten[a]

* corresponding author: Cristian Sabau: cristian.sabau@ltu.se

[a] Luleå Univ. of Technology, Dept. of Civil, Environmental and Natural Resources Engineering, SE-97187, Luleå, Sweden

[b] Northern Research Institute – NORUT, Rombaksveien E6-47, N-8517 Narvik, Norway

[c] Technical Univ. of Denmark, Dept. of Civil Engineering, Building 118, DK-2800 Kgs. Lyngby, Denmark

Abstract

The allowable strain in fibre reinforced polymers reinforcement is limited by design codes to avoid debonding. The near-surface mounted (NSM) reinforcement technique has been proven to produce better anchorage behaviour compared to externally bonded reinforcement solutions. However, NSM solutions do not always eliminate debonding issues, with concrete cover detachment (CCD) typically occurring in RC beams strengthened for flexure. This experimental study investigated the efficiency of side mounted (S) compared to bottom mounted (B) NSM bars to prevent CCD. The experimental results were compared to models available in the literature that predict the observed failure modes and the crack spacing in the NSM anchorage zone. Compared to B-NSM, the S-NSM solution was successful in avoiding brittle CCD failure and showed increased rotational capacity and energy dissipation at failure. Existing CCD debonding models were found to be conservative.

Keywords: debonding; concrete cover detachment; crack spacing; non-contact optical measurements; strain analysis; CFRP; NSM

1. Introduction

Repair and strengthening with fibre-reinforced polymers (FRPs) is a well-established rehabilitation method in the construction industry, with numerous design guidelines available worldwide (e.g. ACI 440.2R [1], CSA S806 [2], CNR-DT200R1 [3], Fib Bulletin 14 [4], [5]) and others soon to be introduced, such as [6].

Flexurally-designed reinforced concrete (RC) beams can fail because of yielding of the tension reinforcement, concrete crushing, or shear flexure. Two of the most common flexural strengthening methods are externally bonded reinforcement (EBR) and near-surface mounted reinforcement (NSM). In both cases, the FRP reinforcement is bonded to the tension side of the element. With the EBR technique, fabrics or laminates, are adhesively bonded directly to the concrete surface whereas, with the NSM technique, FRP bars or lamella are inserted into grooves cut in the element's concrete cover. When RC members are strengthened with FRP, additional failure modes are possible, namely: (a) concrete cover detachment (CCD), (b) end interfacial debonding, or (c) intermediate crack debonding (ICD) [7]. Sudden debonding failure modes were observed in experimental investigations when EBR strengthening was used [8, 9]. This phenomenon usually happens before reaching the tensile strength of the fibres, thus hindering the utilisation of the FRP to the maximum capacity.

The NSM technique was, to the authors' knowledge, first applied in the mid 90-ties for strengthening of a RC cable stayed bridge in Uddevalla, Sweden. Considerable research on NSM strengthening solutions [8-19] has since been carried out. Compared to EBR, the NSM technique provides increased interfacial stress capacity [8-10], due to a larger bond surface and confinement provided by the surrounding concrete [9, 19]. Although the FRP utilisation is increased, debonding failure modes are not avoided.

Current design codes provide special requirements regarding CCD. For example, ACI 440.2R [1] specifies that transversal anchors should be provided at the FRP bar cut-off section if the shear force in the section is more than 67% of the shear strength of the concrete section. Similarly, CNR-DT200R1 [3] recommends the use of anchorage devices such as FRP U-wraps [20] or NSM strips [21]. However, for use in practice, the performance of such solutions needs to be determined experimentally.

In bottom mounted NSM (B-NSM) strengthened beams, CCD is likely to occur if the NSM is terminated at a distance (Δl) from the support. For example, CCD was reported for relatively large cut-off lengths (Δl=200mm) [11, 13] but also for small cut-off lengths (Δl=50 mm) [12].

To the authors' knowledge, only one study was carried out on RC beams strengthened with side mounted NSM (S-NSM), reported in Hosen et al. [22] and Shukri et al. [23], and showed that the S-NSM technique is effective for strengthening RC beams in flexure, in terms of serviceability and ultimate load. The beams were strengthened with steel and carbon FRP (CFRP) rods of 8, 10, and 12 mm diameter. The S-NSM technique produced a significant increase in flexural capacity and cracking load with respect to the reference beams. However, beams strengthened with 12 mm diameter steel and CFRP bars failed due to concrete cover detachment. Shukri et al. [23] further investigated the influence of existing cracks on the performance of CFRP strengthened beams. It was found that pre-cracking slightly decreased the beams' ultimate strength and increased beams' rigidity, however, failure modes remained unchanged.

Often, access to the soffit of RC beams in need of strengthening is limited. Examples of such cases are: a) beams part of a road crossing bridge; b) beams part of a building's structure directly above industrial equipment; and c) beams or spandrels created by cutout openings in RC walls. In such cases, when: a) the road is to remain open; b) the industrial equipment is to remain operational; and c) strengthening of the beam is desired before cutting out the opening; the [more usual] B-NSM technique becomes problematic to apply and the S-NSM technique could be used in instead.

Despite the above-mentioned advantages of S-NSM over B-NSM, the efficiency of S-NSM can be limited by the shorter lever arm in comparison to the B-NSM technique and the limited amount of additional reinforcement that can be provided to the sides of the beams. However, currently no direct comparison has been reported within the available literature. Moreover, the bond behaviour of S-NSM strengthen RC beams is largely unexplored, and, as suggested in Shukri et al. [23], investigations are required to evaluate the effect the bonded length on the effectiveness of the S-NSM technique.

The experimental study, presented in this paper, investigated the efficiency of the S-NSM technique compared to B-NSM, with varied bonded lengths, in terms of ultimate capacity, crack distribution, stiffness, and failure modes. In this study, a 3D optical deformation measurement system Aramis 5M [24], that utilises the digital image correlation (DIC) technique, was used to measure deformations and identify cracks in the NSM anchorage area. The experimentally obtained crack spacing was compared to predictions using existing analytical formulas, and was used to evaluate the performance of existing debonding models.

2. Experimental programme

The experimental programme consisted of seven RC beams, each with a length of 4000 mm and a 200 × 300 mm rectangular cross section (Fig. 1). One beam was tested as a reference specimen; the other six beams were strengthened using different FRP configurations. The longitudinal reinforcement consisted of two 16 mm diameter deformed steel bars, which were placed at both the top and bottom part of the cross section, see Fig. 1. Shear reinforcement consisted of steel stirrups made of deformed steel bars with a nominal diameter of 10 mm, uniformly spaced at 75 mm.

The primary test variable was the placement of NSM (S-NSM vs B-NSM). In all cases, two CFRP bars were used to strengthen the specimens. To produce a CCD, the CFRP bars ended at a distance Δl from the beam's support.

B-NSM beams are denoted B300, B250 and B200 which corresponds to cut-off lengths (Δl) 300, 250 and 200 mm, respectively. S-NSM beams are denoted S300, S250 and S200 which corresponds to values of Δl 300, 250 and 200 mm, respectively. Δl was varied only at one end, north (see Fig. 1), to facilitate CCD failure only in one end, thus making it possible to monitor the area expected to fail. At the other end of the beam, the CFRP bars were extended over the support up to the beam's end.

The NSM groove size was 1.5 times the bar's size, as per ACI 440.2R [1]. For B-NSM strengthened beams, the distance between grooves (i.e. 80 mm) was larger than twice the depth of the groove (i.e. 30 mm). The clear edge distance was 15 mm for all strengthened beams, which was smaller than recommended by ACI 440.2R [1]. However, this was chosen to minimise the difference in effective depth between the B-NSM and S-NSM strengthened beams.

2.1 Material properties

The concrete compressive strength was determined from six cubes with standard sizes according to the procedure described in [25]. The average cube compressive strength (f'_c) was 62.6 MPa equivalent to 50 MPa concrete cylinder compression strength (f_c), according to EC 2 [6]. The average yielding strength (f_y) and yielding strain (ε_y) of the longitudinal reinforcement were 578 MPa, and 2.79‰, respectively, determined according to SS-EN ISO 6892-1 [26].

Rectangular (10 x 10 mm) CFRP bars (StoFRP Bar IM 10 C) and epoxy-based adhesive (StoPox SK 41) were used. The CFRP bars had 3300 MPa nominal tensile strength and 210 GPa modulus of elasticity. The adhesive had 12 MPa shear strength and 2GPa modulus of elasticity. CFRP and adhesive material properties were taken according to the manufacturer's specifications.

2.2 Test set-up and instrumentation

The beams were loaded in a four-point bending set-up (see Fig. 1) with a span L_0 of 3600 mm, using displacement control at a loading rate of 0.6 mm/min up to failure. Load (P), midspan deflection (δ), steel strain (ε_s), and CFRP strain (ε_f) were measured during the loading. Two displacement transducers were used to monitor δ, one at each lateral side of the beam. The strains in the flexural steel and CFRP reinforcement were recorded with strain gauges placed at the midspan, one on each reinforcement bar.

DIC was used to measure full field deformations and identify cracks in the anchorage zone on the north side of the beam. DIC is a technique that uses digital camera images to measure shape and displacement, and requires a contrast pattern to be able to determine the displacement of subsets of the analysed images from the initial undeformed stage to the subsequent deformed stages [27]. The images were acquired with two cameras having 2448 x 2050 pixel resolution and equipped with 12 mm focal length lenses.

The positioning of the two cameras relative to the measured surface and to each other is shown in Fig. 2. The cameras were mounted on a rigid crossbar at a 25° angle and spaced 600 mm apart. The crossbar was placed on a tripod positioned one metre from the measured surface. For the S-NSM beams, the cameras were placed next to the beam, perpendicular to the monitored area while for B-NSM beams, the cameras were placed below the level of the soffit of the tested beams. They were not placed directly under the beam, to avoid damage when the beam failed. This resulted in a 60° angle between the direction of the cameras and the measured surface. Images were acquired at a rate of one a second, and the applied load was recorded for each set of images.

3. Test results

The overall behaviour of the tested specimens was measured in terms of load-deflection response, failure mode, steel and CFRP reinforcement response, and bending stiffness. In addition, CCD of the NSM was investigated through a strain analysis by means of DIC measurements. Table 1 shows a summary of the test results for all specimens.

To compare the performance of B-NSM and S-NSM strengthening, the following load levels were identified from experimental tests and are shown in Table 1: (1) first crack P_{cr}, (2) steel yielding load, P_y, and (3) ultimate load, P_u, for which the corresponding deflection, δ_u and maximum strain in the CFRP bars, ε_{fu}, are indicated. It should be noted that P_{cr} was determined based on slope changes in the P-δ responses and P_y was determined based on strain gauge measurements. Table 1 also shows the energy dissipation at failure, E_d, computed as the area under the P-δ graph for each beam, and the bending stiffness of the beam before the yielding of the steel reinforcement K, computed as the slope of the P-δ curve between the cracking (P_{cr}) and yielding (P_y) loads, respectively.

3.1 Reference beam

A typical trilinear response was observed for the reference beam from which the concrete cracking, and steel yielding points could be identified (see Fig. 3). The beam failed by yielding of the bottom steel reinforcement followed by concrete crushing of the top of the cross section.

3.2 Beams strengthened with B-NSM

Compared to the reference beam, the B-NSM strengthened beams exhibited a significant increase in the yielding load (117 – 128% increase) and ultimate load (122 – 136% increase), see Table 1. Fig. 3 shows the P-δ response of B-NSM strengthened beams compared to the reference beam. Up to P_{cr}, the stiffness of B-NSM strengthened beams was identical to that of the reference. Between P_{cr} and P_y, the stiffness of the strengthened beams was 65 – 76% higher. After P_y, the P-δ became nonlinear, with the bending stiffness slowly decreasing up to failure (Fig. 3).

Thinner flexural cracks were observed compared to the reference beam. However, due to stress concentrations, inclined cracks appeared from the NSM cut-off point. The cracks continued to open until the concrete cover was detached together with the CFRP bars (see Fig. 4). Failure occurred by CCD at the level of the steel reinforcement starting from the CFRP bars' cut-off point, on the northern side, see Fig. 4. The observation was identical for all B-NSM beams, regardless of their cut-off length. A slight increase in the maximum load was observed with a decrease of Δl (see Table 1). The energy dissipation at failure was 41 – 73% higher than that of the reference beam. The maximum strain in the CFRP bars was between 45% and 47% of ε_{fu}.

3.3 Beams strengthened with S-NSM

Compared to the reference beam, S-NSM strengthened beams exhibited a significant increase in the yielding load (83 – 98% increase) and ultimate load (122 – 127% increase), see Table 1. Fig. 5 shows the load-deflection (P-δ) response of S-NSM beams compared to the reference beam. The cracking load, P_{cr}, of specimen S300 was not recorded. Due to a malfunction in the data acquisition system, the test was stopped at a load level of 85 kN. The beam was then unloaded and reloaded, thus the initial part of the response differs to the other strengthened beams. Up to P_{cr}, the stiffness of S-NSM strengthened beams was identical to that of the reference. Between P_{cr} and P_y, the stiffness of the strengthened beams was 46 – 76% higher. After P_y, the bending stiffness decreased up to failure. Failure occurred due to concrete crushing at the top side of the beam, close to the south load application point (as shown in Fig. 6). ICD of the CFRP bars occurred only after the maximum load was reached, while the compressed concrete was still crushing. This debonding started at a flexural-shear crack with approximately 45° inclination. The debonding process ended when the CFRP slipped within the concrete groove (see Fig. 6). This behaviour was identical for all S-NSM strengthened beams. The maximum strain in the CFRP bars was between 51% and 54% of their ε_{fu}, as shown in Table 1.

4. Performance comparison between B-NSM and S-NSM

4.1 Loads and failure mode

Fig. 7 shows the comparison of the load-deflection response of B-NSM and S-NSM strengthened beams having the same Δl. In general, compared to S-NSM beams, B-NSM beams showed higher cracking loads (13%), bending stiffness (14%) and yielding loads (23%). These differences are due to the location of the CFRP bars, specifically the larger effective depth for B-NSM beams compared to S-NSM beams.

B-NSM strengthened beams exhibited a brittle CCD at the north anchorage side, whereas the S-NSM strengthened beams showed a more ductile failure by concrete crushing followed by ICD at the south end of the beam. The reason S-NSM beams did not fail by CCD at the north anchorage side can be attributed to the location of the CFRP bars relative to the flexural steel reinforcement (see Fig. 8). The concrete between the steel reinforcement and the NSM is subjected to tensile and shear stresses induced by the force transferred from the NSM to the end anchorage zone (F_f) [28]. Tensile stresses result from the moment $M_c = F_f \cdot l_c$, see Fig. 8. The distance l_c is defined as the distance between the NSM and the possible failure plane. For B-NSM, the failure plane is located at the lower level of the flexural steel reinforcement, whereas for S-NSM, a possible failure plane is located above the level of the internal reinforcement (see Fig. 8);

this aspect is further discussed in Section 4.2.3 End anchorage crack pattern. For B-NSM, l_c promotes CCD, whereas for S-NSM, l_c leads to considerably lower tensile stresses. This would suggest that CCD is not likely to occur in S-NSM strengthened beams. However, the experiments reported in [22, 23] prove the opposite.

While similar ultimate loads were obtained for B-NSM and S-NSM strengthened beams with the same Δl, the deflection at failure was 31 – 46% higher for S-NSM strengthened beams. Comparing energy dissipation at failure, beams S300, S250 and S200 had 125%, 77%, and 62% higher E_d than beams B300, B250, B200, respectively. Thus, B-NSM strengthened beams have a higher bending stiffness overall while S-NSM strengthened beams have a higher ductility and rotational capacity.

4.2 Strain analysis

4.2.1 Load-strain response

Compared to B-NSM beams, S-NSM beams' steel and CFRP reinforcement strains (Fig. 9s and Fig. 9b, respectively) were initially slightly higher and lower, respectively. This is expected due the difference between the effective depth of the CFRP reinforcement for the two systems. After P_y however, the CFRP strain for S-NSM beams was higher. For beam S200, the steel strain gauges malfunctioned at approximately 125 kN applied load.

The maximum CFRP strain in the S-NSM beams was 11 – 18% higher compared to B-NSM beams. Thus, the CFRP reinforcement had a higher utilisation ratio (0.50 to 0.54 ε_{fu}) in the S-NSM beam configuration compared to the B-NSM beam configuration (0.43 to 0.46 ε_{fu}).

4.2.2 End anchorage longitudinal crack spacing

The distribution of major principal strains in the monitored areas preceding failure is shown in Fig. 10. For B-NSM beams, only the soffit of the beam was monitored while for S-NSM beams, only the side of the beam was monitored. According to the coordinate system shown in Fig. 2, the strain maps in Fig. 10 are given relative to the planes *xy* and *xz* for B-NSM and S-NSM beams, respectively. In all cases, *x* represents the longitudinal axis of the beam with zero being the location of the north support. Axis *y* represents the thickness of the beams, with zero being the side of the beam. Axis *z* represents the height of the beam, with zero being the soffit of the beam. It should be noted that the strains shown in Fig. 10 greatly exceed the realistic tensile strains expected in the concrete. However, the presented strain distribution is useful for evaluating crack initiations, paths, distribution and spacing. The scale representation of deformation in this case was chosen such that red areas indicate fully formed cracks. For both B-NSM and S-NSM strengthened beams, crack spacing was measured at the bottom face of the beam.

The minimum distance between two consecutive cracks (i.e. minimum crack spacing) observed for B-NSM beams was approximately 50 – 60 mm. The maximum distances between two consecutive cracks (i.e. the maximum crack spacing) of 80, 100, and 110 mm were observed for B300, B250 and B200, respectively, closest to the cut-off point. The maximum crack spacing in this case was observed to be approximately twice the minimum spacing. Moreover, Fig. 10 indicates that the cut-off length Δl possibly influences the crack spacing, a parameter currently not accounted for by existing equations for predicting crack spacing in B-NSM beams [29-31].

Larger crack spacing was observed for S-NSM than for B-NSRM beams, being 185, 180 and 170 mm for S300, S250 and S200, respectively. This suggests that the location of the NSM (bottom or side) influences the stress distribution in the anchorage zone and consequently the crack patterns.

4.2.3 End anchorage crack pattern

In S-NSM strengthened beams, horizontal cracks were observed above the NSM (see Fig. 10), also above the flexural steel reinforcement (see Fig. 8). Cracks start as flexural-shear cracks and propagate towards the cut-off point, indicative of CCD. This differs from previous reported observations for S-NSM strengthened beams [22] and B-NSM strengthened beams [11-13], where the CCD was initiated as a vertical crack at the CFRP cut-off point, propagating below the level of the flexural steel reinforcement towards the middle of the beam.

In S-NSM beams, the possible debonding plane was located above the flexural steel reinforcement (see Fig. 8) and, assuming it propagates as the same level over the thickness of the beam (as in the case of B-NSM [11-13]), the shear reinforcement intersected by the failure plane prevented CCD. Therefore, in the tested S-NSM strengthened beams, the failure plane was not fully established.

5. Comparison of experimental and analytical results

The simplified analytical model proposed by An et al. [32] for rectangular beams was used to calculate sectional stresses and deformations. The model is based on the following assumptions: (1) linear strain distribution through the full depth of the beam; (2) small deformations; (3) the concrete does not carry tensile stresses after cracking; (4) shear deformations are not considered and (5) there is a perfect bond between the internal steel reinforcement and concrete, and NSM and the concrete. The stress-strain relationship for CFRP reinforcement is linear elastic. The stress-strain relationship for internal steel reinforcement is assumed elastic-perfectly plastic. Hognestad's [33] parabola of an idealised stress-strain curve was used for concrete in compression.

The strain and stresses in the FRP bars and steel reinforcement, as well as curvature at midspan, were calculated using an incremental deformation technique, in which the strain in the extreme concrete fibre is increased from 0 to 3000με, considered the ultimate useful concrete strain. The strain in the steel and FRP reinforcement was calculated for each increment from a cross sectional analysis to satisfy the force equilibrium and deformation compatibility conditions. The moment and curvature were computed using the moment-curvature relationship, starting from the strain in the extreme concrete fibre. Finally, the load-deflection response was derived. An automated calculation procedure was developed to carry out the calculations. A good agreement can be seen in terms of applied load-midspan displacement between the model and the experimental tests (Fig. 11).

The bond between internal and NSM reinforcement and concrete was not modelled explicitly. Instead, for CCD, the models proposed by Al-Mahmoud et al. [28] and Teng et al. [34] were used to predict the failure load of strengthened specimens. According to a recent assessment of current guidelines [1-3], current formulations for NSM interfacial debonding provide conservative results with limited accuracy [35]. Instead, in this study, the model proposed by Mohamed Ali et al. [36] was used to predict the interfacial debonding failure load.

5.1 Interfacial debonding model

Mohamed Ali et al. [36] proposed two models for the debonding of NSM, using linear and bilinear interfacial bond characteristics, respectively. Both models were shown to have good accuracy compared to experimental data obtained from pull-out tests, especially for predicting the debonding load [36]. The simplified linear model is a closed-form solution, applicable to ICD. The maximum interfacial shear stress and slip are obtained from:

$$\tau_f = 0.54\sqrt{f_c}\,h_f^{0.4} b_f^{0.3} \tag{1}$$

$$\delta_f = 0.78\left(\frac{f_c^{0.27}}{b_g^{0.3}}\right) \tag{2}$$

where f_c is the concrete compressive strength, h_f and b_f are the height and width of the FRP reinforcement, respectively, and b_g is the groove size.

For cases where the anchorage length is longer than the effective bond length, the NSM debonding strength is:

$$F_{deb}^{ICD} = \frac{\tau_f L_{per}}{\lambda} \tag{3}$$

where L_{per} is the total perimeter of the FRP-concrete interface at the end of L_e and λ is a constant:

$$\lambda = \sqrt{\frac{\tau_f L_{per}}{\delta_f E_f A_f}} \tag{4}$$

where E_f and A_f are the Young modulus and the total cross sectional area of the FRP reinforcement, respectively.

The FRP strain associated to F_{deb}^{ICD} can be determined as:

$$\varepsilon_f^{ICD} = \frac{F_{deb}^{ICD}}{A_f E_f} \quad (5)$$

The moment in the cracked section $M(x_{cr})$ where debonding is initiated can be determined from the cross section analysis starting from ε_f^{ICD}.

5.2 Concrete cover detachment model

Teng et al. [34] proposed a strength model for predicting the strain in the FRP at the critical cracked section when CCD occurs:

$$\varepsilon_f^{CCD} = 10^4 \cdot \beta_{cs}\beta_{AE}\beta_{bod} b_{clear}\sqrt{f_c} \quad (6)$$

$$\beta_{cs} = \left(\frac{4.5}{w_c^{0.3}} - \frac{l_c}{w_c}\right)\left(\frac{w_c}{100} - 0.1\right) \quad (7)$$

$$\beta_{AE} = \frac{1}{(A_f E_f)^{0.9}} \quad (8)$$

$$\beta_{bod} = \left(\frac{b_{clear}}{D_t}\right)^{0.1} \quad (9)$$

where D_t is the sum of the diameter of all tension steel reinforcement bars placed closest to the NSM, and $b_{clear} = b - D_t$, the clear width of the beam. In Eq. 6, β_{cs} accounts for the combined effect of l_c and w_c; β_{AE} accounts for the influence of the FRP axial rigidity and β_{bod} accounts for the effect of reinforcement size and number. Starting from ε_f^{CCD}, the moment in the critical cracked section can be determined from cross section analysis. According to Teng et al. [34], the model gives better predictions compared to the other available models suggested by [28, 37]. For the sake of brevity, the models proposed by [28, 37] are not shown here.

5.3 Evaluation of crack spacing

The crack spacing in the anchorage zone is of great importance for predictions based on the concrete tooth model. All available CCD debonding models [28, 34, 37] were developed using crack spacing values obtained from experimental observations [28] or from finite element analysis [34]. According to De Lorenzis and Nanni [31], the minimum crack spacing in NSM strengthened beams can be calculated by:

$$s_c^{min} = \frac{A_e f_{ct}}{u_s \sum O_s + \tau_f \sum O_f} \quad (10)$$

where A_e is the area of concrete in tension, $u_s = 0.28\sqrt{f'_c}$ and is the local bond strength of the steel reinforcement, τ_f is the bond strength of the NSM, $\sum O_s$ is the total perimeter of the internal steel reinforcement, and $\sum O_f$ is the total perimeter of NSM. Zhang et al. [30] proposed a similar equation for s_c^{min}, however $u_f = 0.28\sqrt{f'_c}$ and the total NSM groove perimeter are used instead of τ_f and $\sum O_f$, respectively. Other equations for predicting the crack spacing of NSM strengthened beams have been proposed by Piyasena et al. [29]. For the sake of brevity, they are not shown here.

Table 2 shows a summary of the observed minimum crack spacing (w_c^{min}) in the anchorage zone using DIC (see Fig. 10) and the values obtained using the three mentioned models. It should be noted that all models were developed based only on B-NSM strengthened beams and neither of them explicitly accounted for the influence of d_f or Δl.

Models by Zhang et al. [30] and De Lorenzis and Nanni [31] yielded results that were in better agreement with the minimum crack spacing observed for B-NSM beams, albeit the latter slightly overestimated, while values provided from the model by Piyasena et al. [29] were comparable with the ones observed for S-NSM beams. Perhaps the crack spacing of S-NSM beams can be evaluated using the same equation as that for internally reinforced beams, adapted to account for the mechanical and bond properties of NSM.

5.4 Comparison with test results

For four-point bending, the moment at the critical crack location (x_{cr}) can be obtained as:

$$M(x_{cr}) = M\frac{x_{cr}}{a_v} \tag{11}$$

where M is the moment in the maximum moment region (i.e. between the load application point) and a_v is the shear span of the beam. From static equilibrium conditions, it follows that the associated total force in the actuator is:

$$P = 2\frac{M}{\alpha_L L_0} = 2M(x_{cr})\frac{1}{x_{cr}} \tag{12}$$

where, for CCD debonding, x_{cr} can be estimated as $\Delta l + w_c$ and for ICD can be considered as being $a_v - d_f/2$.

Table 3 shows a summary of the experimentally and analytically determined maximum loads associated with CCD and ICD debonding failure. The predicted ICD debonding loads for B-NSM beams were higher than the observed maximum load, which is in good agreement with the observed failure modes, as B-NSM beams failed by CCD. The predicted CCD debonding loads for B-NSM (calculated using [34]) and ICD debonding loads for S-NSM (calculated using [36]) are shown in Fig. 12, respectively, together with the experimental and theoretical load-deflection responses.

Based on the experimental results for B-NSM beams, the models by Teng et al. [34] and Hassan and Rizkalla [37] show similar performances, having average predicted-to-tested ratios of 0.67 and 0.66, respectively, whereas the model by Al-Mahmoud et al. [28] was the most conservative, having an average predicted-to-tested ratio of 0.52. The model by [37] was found to have the lowest coefficient of variation (COV), 0.03, whereas those by Teng et al. [34] and Al-Mahmoud et al. [28] had 0.20 and 0.3 COV, respectively. In all cases, the experimentally determined crack spacing for each beam was used as an input parameter. This indicates that the former two models have a high sensitivity to the parameter Δl in the range investigated in this study.

The ICD model proposed by Mohamed Ali et al. [36] predicted the capacity of S-NSM beams with good accuracy, having an average of predicted-to-tested ratio of 1.01 and with 0.01 COV (see Fig. 12b and Table 3).

For S-NSM beams, the models by Teng et al. [34] and Hassan and Rizkalla [37] provided average predicted-to-tested ratios of 1.01 and 0.55, with 0.19 and 0.07 COV, respectively. While CCD debonding did not occur, results suggest that models by both Teng et al. [34] and Hassan and Rizkalla [37] provided conservative predictions. However, experimental tests where the CCD failure mode for S-NSM beams occurs are necessary to determine the influence of shear reinforcement, crack spacing in the anchorage zone, and NSM cut-off distance on the debonding capacity.

6. Conclusions

This paper describes the results of experimental tests carried out on six RC concrete beams strengthened with NSM CFRP reinforcement at different locations. The NSM were placed at the bottom of the beam (B-NSM) and at the side of the beam (S-NSM). The NSM was provided with different anchorage lengths. Strains and crack patterns in the anchorage zone were recorded using a 3D-DIC deformation measurement system. These observations provided insight into the concrete cover detachment failure mode. The performances of analytical models used to predict the crack spacing in the anchorage zone and the maximum capacity of the strengthened beams were investigated. Based on the findings of this study, the following conclusions can be drawn. An S-NSM strengthening system, when compared to a B-NSM system:

- Provided a similar ultimate load carrying capacity
- Was successful in avoiding concrete cover detachment
- Increased the CFRP strain at failure by 11 to 18%
- Increased the energy dissipation at failure by 1.6 to 2.3 times
- Increased the maximum deflection at failure by 31 to 46%

Moreover, by comparing experimental tests with models, the following conclusions can be drawn:

- The interfacial debonding model by Mohamed Ali et al. [36] predicted, with good accuracy, the intermediate crack debonding failure load of S-NSM strengthened beams
- The crack spacing in the anchorage zone of B-NSM and S-NSM strengthened beams was best predicted with models by Zhang et al. [30] and Piyasena et al. [29], respectively
- Existing CCD debonding models for B-NSM strengthen beams were found to be conservative, and future CCD debonding for S-NSM strengthened beams should consider the influence of the beam’s internal shear reinforcement

Further experimental tests are needed to study concrete cover detachment failure modes in S-NSM strengthened beams. The influence of parameters such as concrete cover thickness, flexural and shear reinforcement ratio, NSM location, and support conditions should be addressed in future studies.

Acknowledgements

The authors wish to thank Mr Oskar Seth and MSc Rewan Eredini for their help in the experimental programme. This work was supported by the European Commission (Contract number MC-ITN-2013-607851) and the Structural Engineering Department of Luleå University of Technology (LTU) through internal funds.

References

[1] ACI 440.2R. Guide for the Design and Construction of Externally Bonded FRP Systems for Strengthening Concrete Structures. Farmington Hills, Michigan, USA: American Concrete Institute; 2017. p. 116.

[2] CSA S806. CSA S806. Design of concrete structures. Toronto, Canada: Canadian Standards Association; 2012.

[3] CNR-DT200R1. Guide for the design and construction of externally bonded FRP systems for strengthening existing structures. Rome, Italy: National Research Council (CNR); 2013.

[4] Fib Bulletin 14. Externally bonded FRP reinforcement for RC structures. Lausanne, Switzerland: Federation for Structural Concrete (fib); 2001.

[5] Täljsten B, Blanksvärd T, Sas G. Handbok för dimensionering i samband med förstärkning av betongkonstruktioner med pålimmade fiberkompositer [Design Guideline for FRP Strengthening of Existing Concrete Structures. In Swedish]. Div. of Structural Engineering, Luleå University of Technology2011.

[6] EC 2. Eurocode 2: Design of concrete structures. Brussels, B-1050, Belgium: European Committee for Standardization (CEN); 2005.

[7] Grace C, Yang Y, Sneed L. Fracture Mechanics Approaches to Debonding Behavior of Reinforced Concrete Members with Externally-bonded Fiber Reinforced Polymer Laminates. ACI Special Publication. 2012;286.

[8] Bilotta A, Ceroni F, Di Ludovico M, Nigro E, Pecce M, Manfredi G. Bond Efficiency of EBR and NSM FRP Systems for Strengthening Concrete Members. Journal of Composites for Construction. 2011;15(5):757-72.

[9] Bilotta A, Ceroni F, Nigro E, Pecce M. Efficiency of CFRP NSM strips and EBR plates for flexural strengthening of RC beams and loading pattern influence. Composite Structures. 2015;124:163-75.

[10] Lundqvist J, Nordin H, Täljsten B, Olofsson T. Numerical analysis of concrete beams strengthened with CFRP : a study of anchorage lengths. In: Proceedings of International Symposium on Bond Behaviour of FRP in Structures : 2005. Conference 2005, Conference 2005. p. 239-46.

[11] Sharaky IA, Torres L, Comas J, Barris C. Flexural response of reinforced concrete (RC) beams strengthened with near surface mounted (NSM) fibre reinforced polymer (FRP) bars. Composite Structures. 2014;109:8-22.

[12] Barros JAO, Fortes AS. Flexural strengthening of concrete beams with CFRP laminates bonded into slits. Cement and Concrete Composites. 2005;27(4):471-80.

[13] Al-Mahmoud F, Castel A, François R, Tourneur C. Strengthening of RC members with near-surface mounted CFRP rods. Composite Structures. 2009;91(2):138-47.

[14] Sas G, Dăescu C, Popescu C, Nagy-György T. Numerical optimization of strengthening disturbed regions of dapped-end beams using NSM and EBR CFRP. Composites Part B: Engineering. 2014;67:381-90.

[15] Bennitz A, Täljsten B, Danielsson G. CFRP strengthening of a railway concrete trough bridge – a case study. Structure and Infrastructure Engineering. 2012;8(9):801-16.

[16] Nordin H, Täljsten B. Concrete Beams Strengthened with Prestressed Near Surface Mounted CFRP. Journal of Composites for Construction. 2006;10(1):60-8.

[17] Täljsten B, Carolin A, Nordin H. Concrete Structures Strengthened with Near Surface Mounted Reinforcement of CFRP. Advances in Structural Engineering. 2003;6(3):201-13.

[18] Enochsson O, Lundqvist J, Täljsten B, Rusinowski P, Olofsson T. CFRP strengthened openings in two-way concrete slabs – An experimental and numerical study. Construction and Building Materials. 2007;21(4):810-26.

[19] Mostakhdemin Hosseini MR, Dias SJE, Barros JAO. Flexural strengthening of reinforced low strength concrete slabs using prestressed NSM CFRP laminates. Composites Part B: Engineering. 2016;90:14-29.

[20] Gonzalez-Libreros JH, Sneed LH, D'Antino T, Pellegrino C. Behavior of RC beams strengthened in shear with FRP and FRCM composites. Engineering Structures. 2017;150:830-42.

[21] Bianco V, Barros JA, Monti G. Bond Model of NSM-FRP Strips in the Context of the Shear Strengthening of RC Beams. Journal of Structural Engineering. 2009;135(6):619-31.

[22] Hosen MA, Jumaat MZ, Islam ABMS. Side Near Surface Mounted (SNSM) technique for flexural enhancement of RC beams. Materials & Design. 2015;83:587-97.

[23] Shukri AA, Hosen MA, Muhamad R, Jumaat MZ. Behaviour of precracked RC beams strengthened using the side-NSM technique. Construction and Building Materials. 2016;123:617-26.

[24] GOM mbH. ARAMIS - Optical 3D Deformation Analysis. 6.3 ed. Braunschweig Germany: GOM mbH; 2008.

[25] EN ISO 12390-3. Testing hardened concrete – Part 3: Compressive strength of test specimens. Brussels, B-1000, Belgium: European Committee for Standardization (CEN); 2009.

[26] SS-EN ISO 6892-1. Metallic materials – Tensile testing – Part 1: Method of test at room temperature. Stockholm, Sweden: Swedish Standards Institute (SIS); 2009.

[27] Reu P. Introduction to Digital Image Correlation: Best Practices and Applications. Exp Tech. 2012;36(1):3-4.

[28] Al-Mahmoud F, Castel A, François R, Tourneur C. RC beams strengthened with NSM CFRP rods and modeling of peeling-off failure. Composite Structures. 2010;92(8):1920-30.

[29] Piyasena R, Loo YC, Fragomeni S. Determination of crack spacing and crack width in reinforced concrete beams. Structural Engineering and Mechanics. 2003;15(2):159-80.

[30] Zhang J, Raoof M, Wood LA. Prediction of peeling failure of reinforced concrete beams with externally bonded steel plates. Proceedings of the Institution of Civil Engineers - Structures and Buildings. 1995;110(3):257-68.

[31] De Lorenzis L, Nanni A. Design procedure of NSM FRP reinforcement for strengthening of RC beams. Fibre-Reinforced Polymer Reinforcement for Concrete Structures: World Scientific Publishing Company; 2012. p. 1455-64.

[32] An W, Saadatmanesh H, Ehsani MR. RC Beams Strengthened with FRP Plates. II: Analysis and Parametric Study. Journal of Structural Engineering. 1991;117(11):3434-55.

[33] E. H. A study of combined bending and axial load in reinforced concrete members. University of Illinois Engineering Experiment Station; 1951. p. 128.

[34] Teng JG, Zhang SS, Chen JF. Strength model for end cover separation failure in RC beams strengthened with near-surface mounted (NSM) FRP strips. Engineering Structures. 2016;110(Supplement C):222-32.

[35] D'Antino T, Limonta A, Pisani MA. Assessment of current guideline formulations for flexural strengthening of reinforced concrete beams using NSM reinforcement. In: Proceedings of 8th International Conference on FRP Composites in Civil Engineering. Hong Kong, China, Conference, Conference 2016.

[36] Mohamed Ali MS, Oehlers DJ, Griffith MC, Seracino R. Interfacial stress transfer of near surface-mounted FRP-to-concrete joints. Engineering Structures. 2008;30(7):1861-8.

[37] Hassan T, Rizkalla S. Investigation of Bond in Concrete Structures Strengthened with Near Surface Mounted Carbon Fiber Reinforced Polymer Strips. Journal of Composites for Construction. 2003;7(3):248-57.

Figure captions

Fig. 1. Test specimen details (units in mm)

Fig. 2. Test setup and location of DIC monitored area with respect to the defined coordinate system

Fig. 3. Load-midspan deflection response of B-NSM beams

Fig. 4. CCD debonding of B-NSM strengthened beams

Fig. 5. Load-midspan deflection response of S-NSM beams

Fig. 6. S-NSM strenghtend beams after failure (concrete crushing and ICD)

Fig. 7 Comparison of load-midspan displacement responses: (a) Δl=300 mm; (b) Δl=250 mm; (c) Δl= 200 mm

Fig. 8 Isolated concrete tooth between the last two adjacent cracks for B-NSM and S-NSM strengthening system

Fig. 9 Load-strain response for (a) steel reinforcement: (b) CFRP bars

Fig. 10 Principal tensile strain distribution on the surface of the north anchorage zone, bottom view for B-NSM (left) and side view for S-NSM (right), relative to the coordinate system (units in mm)

Fig. 11 Comparison between the theoretical and experimentally obtained Load-midspan deflection response

Fig. 12 Experimental and analytical comparison of debonding loads for a) B-NSM (CCD [34]) and b) S-NSM (ICD [36])

Tables

Table 1 Test results

Specimen	Cracking load P_{cr} (kN)	Yielding load P_y (kN)	Ultimate load P_u (kN)	Max. deflection δ_u (mm)	Bending stiffness K (N/mm)	Energy dissipation E_d (kNm)	Max. CFRP strain ε_f (μm/m)
Ref	10.0	54	78	51.0	2643	2.79	-
B300	12.4 (24%)	118 (119%)	173 (122%)	40.6	4644 (76%)	3.94 (41%)	6390 ($0.46\varepsilon_{fu}$)
B250	16.0 (60%)	117 (117%)	178 (128%)	45.7	4355 (65%)	4.69 (68%)	6118 ($0.44\varepsilon_{fu}$)
B200	15.7 (57%)	123 (128%)	184 (136%)	45.7	4555 (72%)	4.82 (72%)	6526 ($0.47\varepsilon_{fu}$)
S300	n.a.	107 (98%)	177 (127%)	59.5	n.a.	n.a.	7114 ($0.51\varepsilon_{fu}$)
S250	14.6 (46%)	99 (83%)	177 (127%)	60.0	3978 (51%)	8.28 (198%)	7244 ($0.52\varepsilon_{fu}$)
S200	13.6 (36%)	102 (89%)	173 (122%)	60.5	3860 (46%)	7.83 (181%)	7568 ($0.54\varepsilon_{fu}$)

n.a. - data not available;
Note: increase relative to reference beam given in parenthesis.

Table 2 Minimum crack spacing in the CFRP anchorage zone

Specimen	s_c^{min} Piyasena et al. [29] (mm)	s_c^{min} Zhang et al. [30]	s_c^{min} De Lorenzis and Nanni [31]	[a)] w_c^{min} (mm)
B300				50
B250				50
B200	137	54	78	60
S300				[b)] -
S250				120
S200				100

[a)] Values from tests
[b)] The stabilised crack region was outside the DIC measured area

Table 3 Experimental and analytical loads of strengthened beams

Specimen	Failure mode	P_{max}^{exp} (kN)	P^{CCD} [34] (kN)	P^{CCD} [37] (kN)	P^{CCD} [28] (kN)	P^{ICD} [36] (kN)	P^{CCD}/P^{exp} [34]	P^{CCD}/P^{exp} [37]	P^{CCD}/P^{exp} [28]	P^{ICD}/P_{max}^{exp} [36]
B300	CCD	173	86	110	56		0.50	0.64	0.32	0.92
B250	CCD	178	116	120	95	189	0.65	0.67	0.53	0.94
B200	CCD	184	157	125	129		0.85	0.68	0.70	0.97
S300	ICD	177	135	90			0.76	0.51		1.02
S250	ICD	177	186	96		174	1.05	0.54		1.02
S200	ICD	173	210	104			1.21	0.60		1.00

CCD Models: Teng et al. [34]; Hassan and Rizkalla [37]; Al-Mahmoud et al. [28];
ICD Model: Mohamed Ali et al. [36]

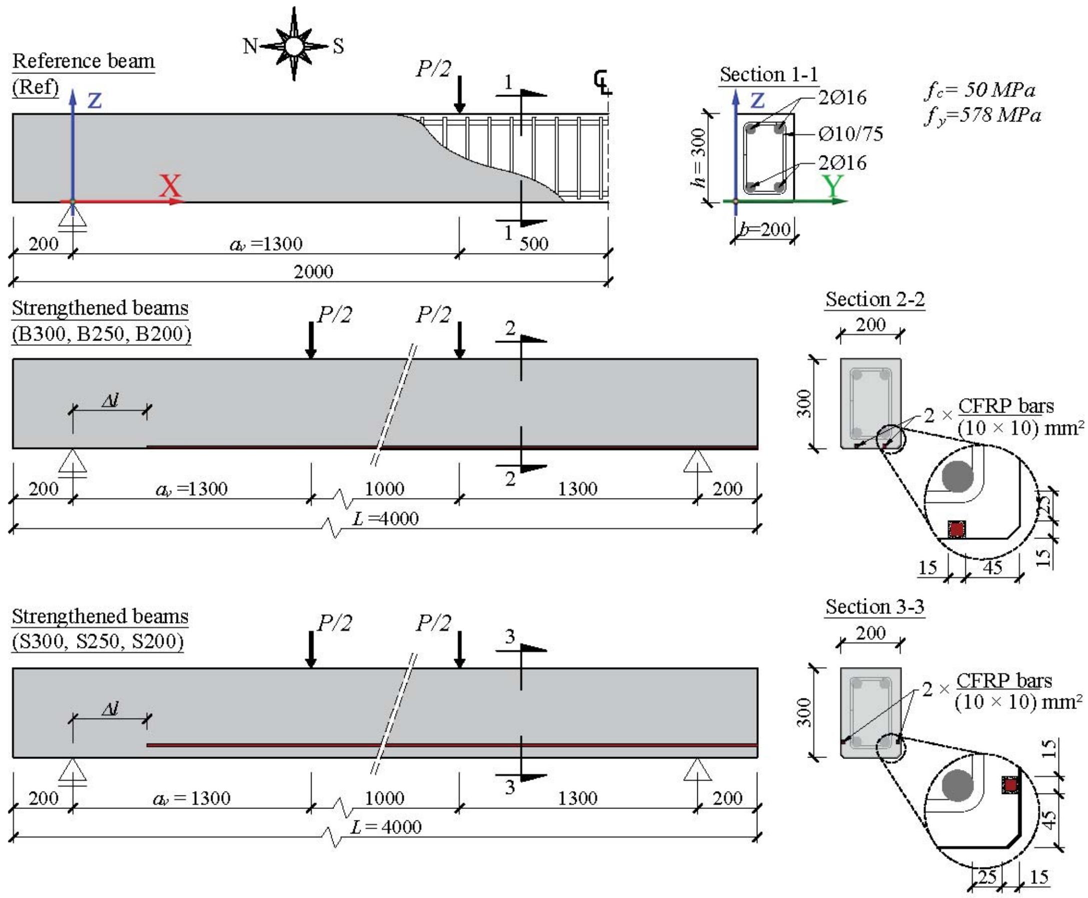

Reference beam
(Ref)
N
S
P/2
Z
X
1
1
Section 1-1
Z
2Ø16
Ø10/75
2Ø16
Y
h = 300
b=200
f_c= 50 MPa
f_y=578 MPa
200
a_v =1300
500
2000
Strengthened beams
(B300, B250, B200)
P/2
P/2
2
2
Δl
200
a_v =1300
1000
1300
200
L =4000
Section 2-2
200
300
2 × CFRP bars
(10 × 10) mm²
25
15
15
45
Strengthened beams
(S300, S250, S200)
P/2
P/2
3
3
Δl
200
a_v = 1300
1000
1300
200
L = 4000
Section 3-3
200
300
2 × CFRP bars
(10 × 10) mm²
15
45
25
15

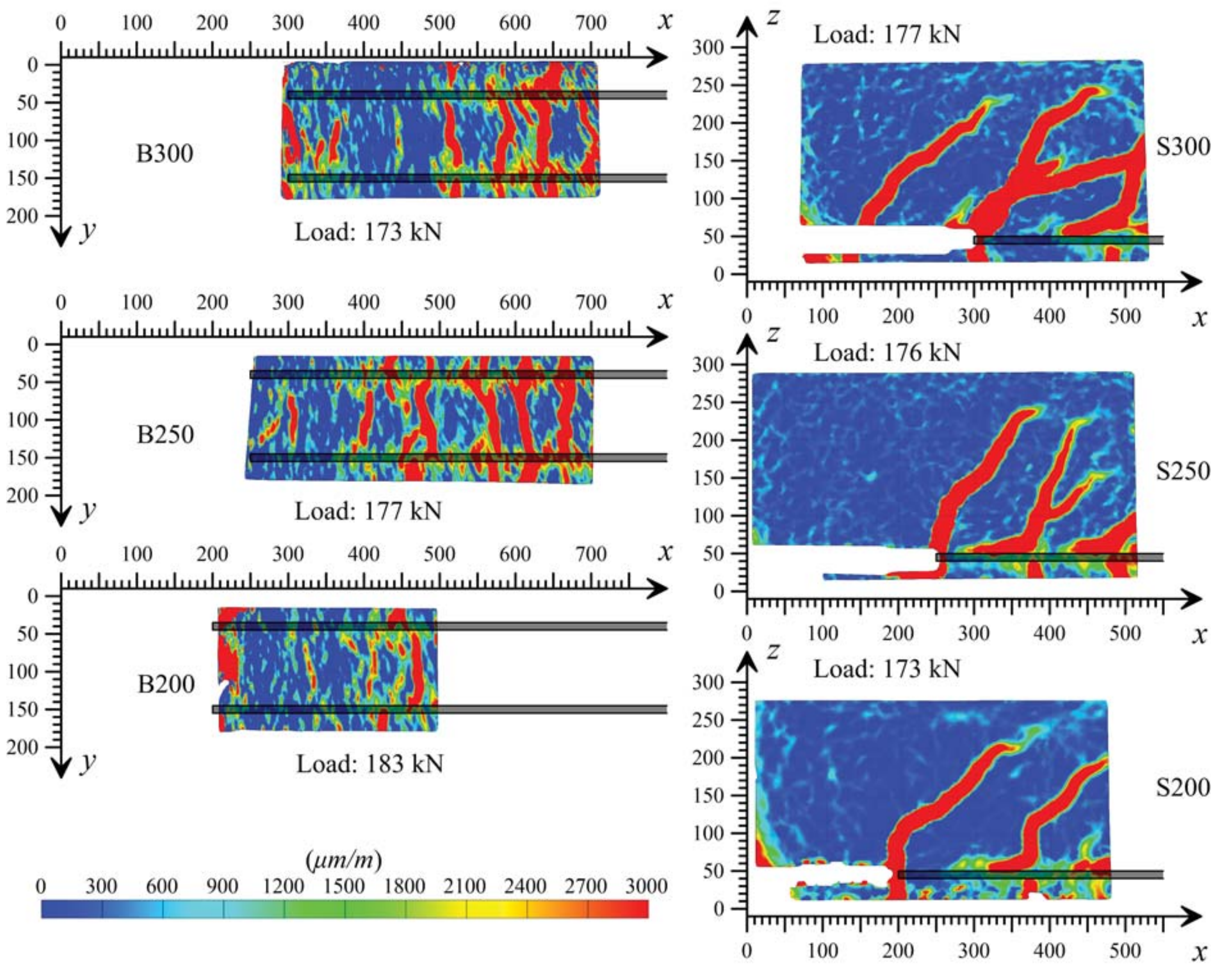

B300
Load: 173 kN
B250
Load: 177 kN
B200
Load: 183 kN
S300
Load: 177 kN
S250
Load: 176 kN
S200
Load: 173 kN
(μm/m)
0 300 600 900 1200 1500 1800 2100 2400 2700 3000
x
y
z

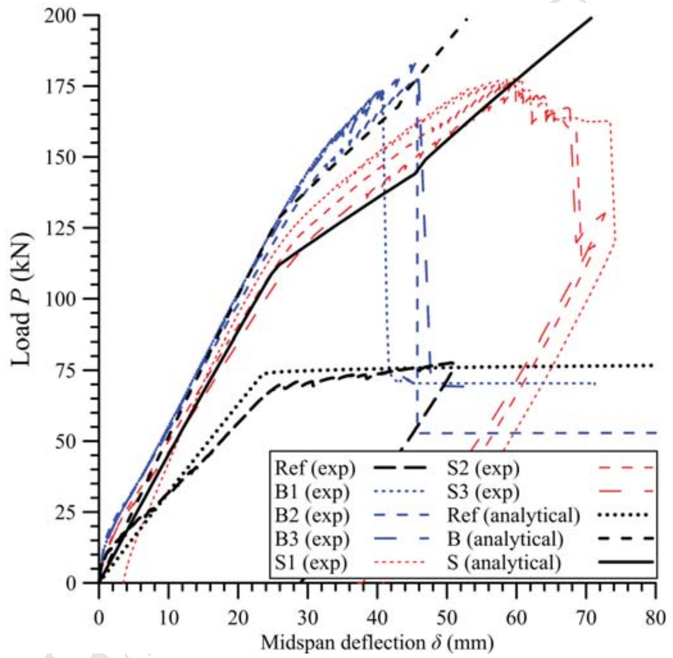
Load P (kN)
Midspan deflection δ (mm)
0
25
50
75
100
125
150
175
200
0
10
20
30
40
50
60
70
80
Ref (exp)
B1 (exp)
B2 (exp)
B3 (exp)
S1 (exp)
S2 (exp)
S3 (exp)
Ref (analytical)
B (analytical)
S (analytical)

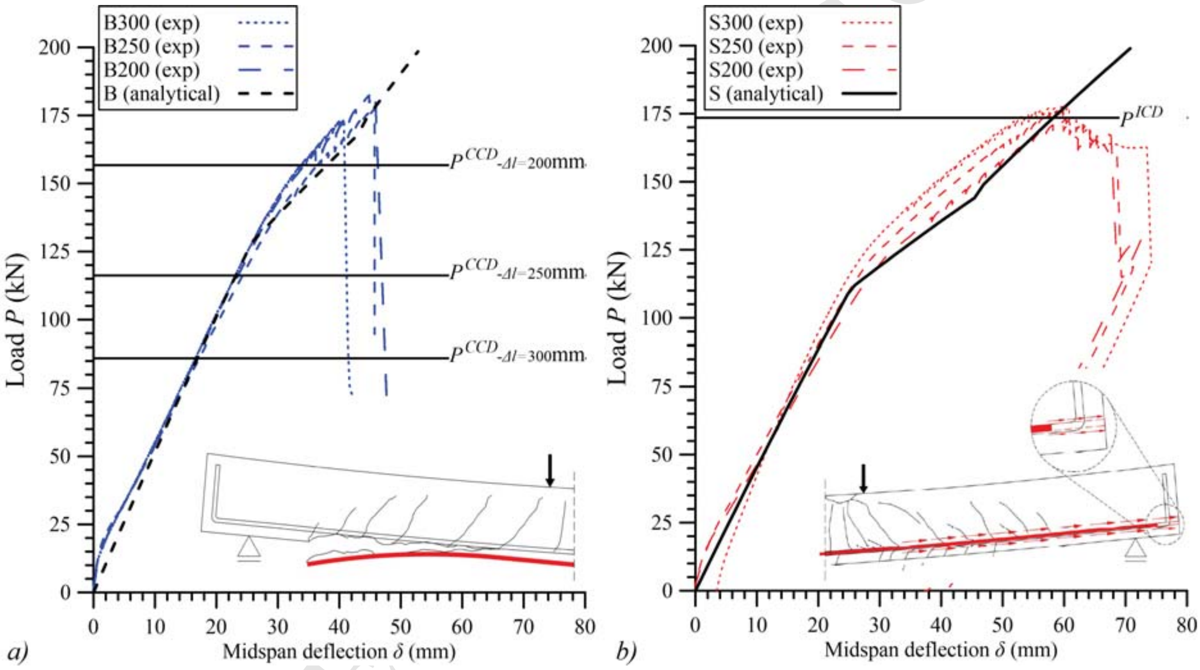

B300 (exp)
B250 (exp)
B200 (exp)
B (analytical)
P^{CCD}-Δl=200mm
P^{CCD}-Δl=250mm
P^{CCD}-Δl=300mm
Load P (kN)
Midspan deflection δ (mm)
a)
S300 (exp)
S250 (exp)
S200 (exp)
S (analytical)
P^{ICD}
Load P (kN)
Midspan deflection δ (mm)
b)

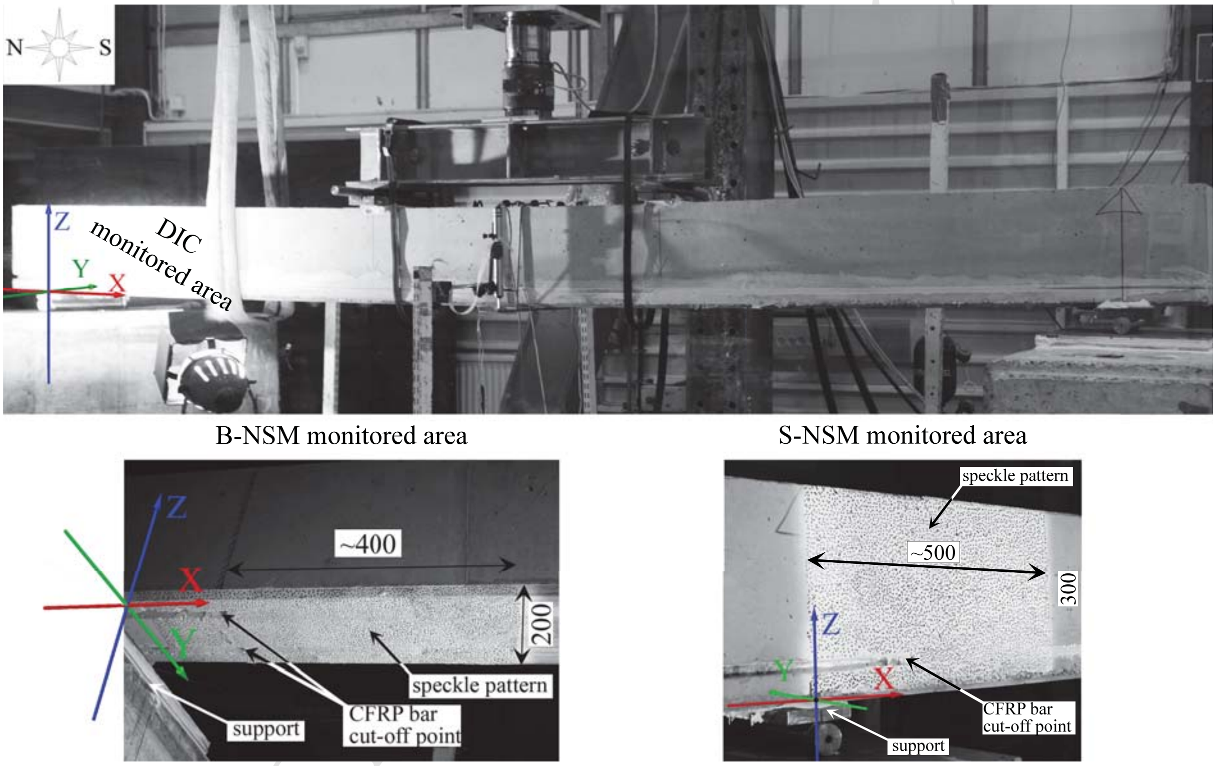

N
S
Z
Y
X
DIC
monitored area
B-NSM monitored area
Z
~400
X
200
Y
speckle pattern
CFRP bar
cut-off point
support
S-NSM monitored area
speckle pattern
~500
300
Z
Y
X
CFRP bar
cut-off point
support

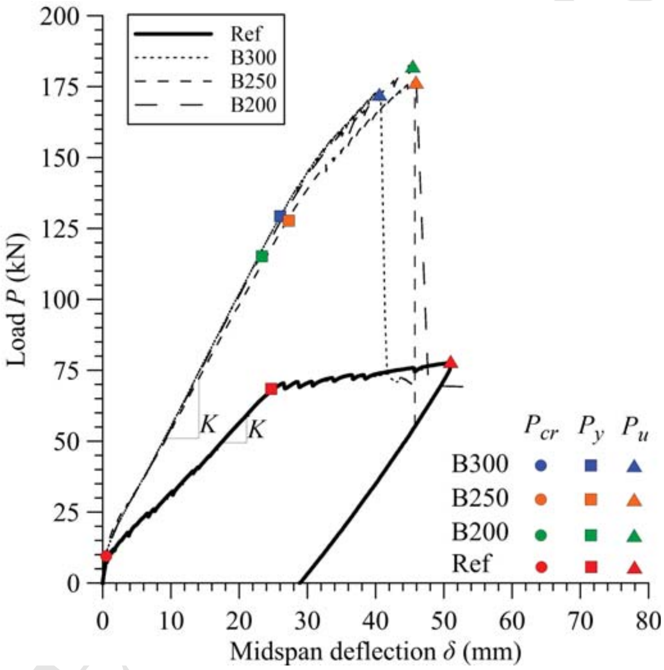

Ref
B300
B250
B200
Load P (kN)
Midspan deflection δ (mm)
K
K
P_cr P_y P_u
B300
B250
B200
Ref
0
25
50
75
100
125
150
175
200
0
10
20
30
40
50
60
70
80

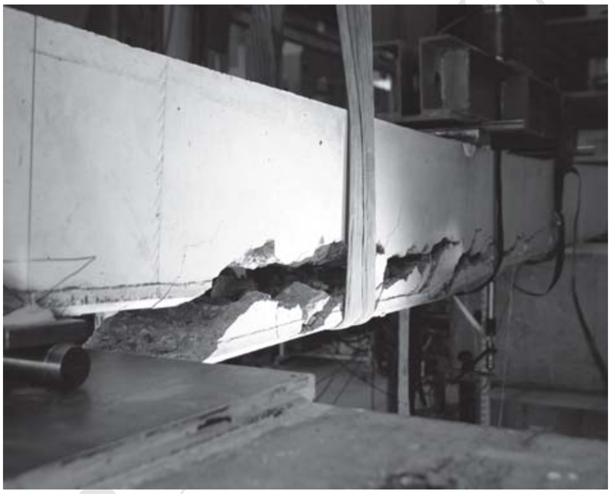

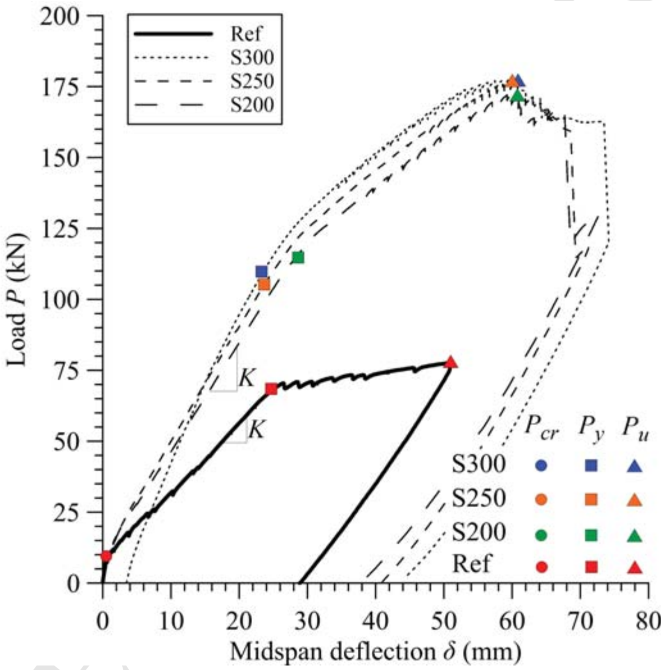

200
175
150
125
100
75
50
25
0
0
10
20
30
40
50
60
70
80
Load P (kN)
Midspan deflection δ (mm)
Ref
S300
S250
S200
K
K
P_{cr} P_y P_u
S300
S250
S200
Ref

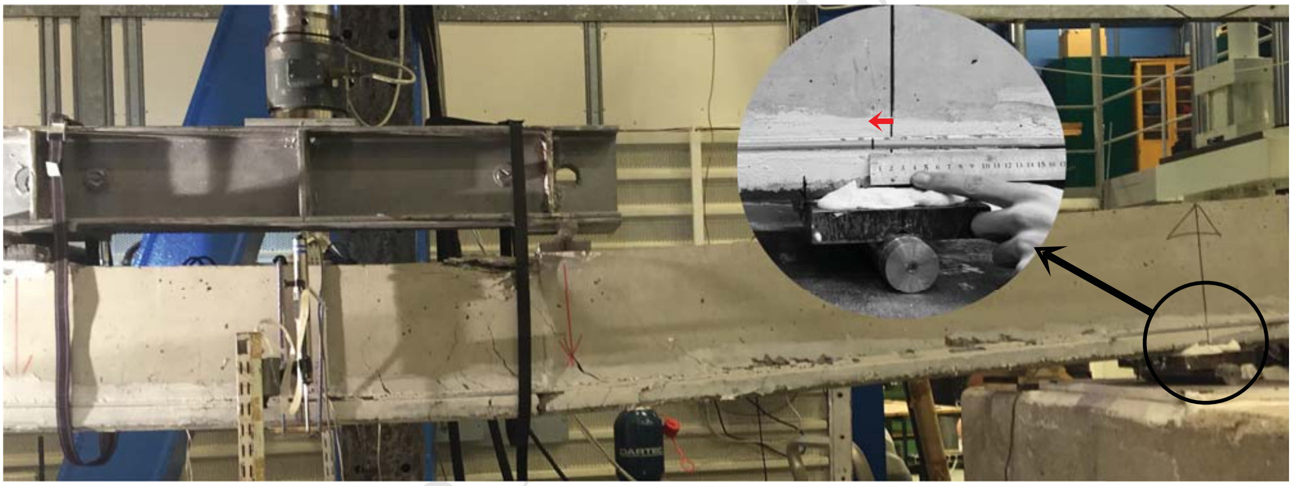

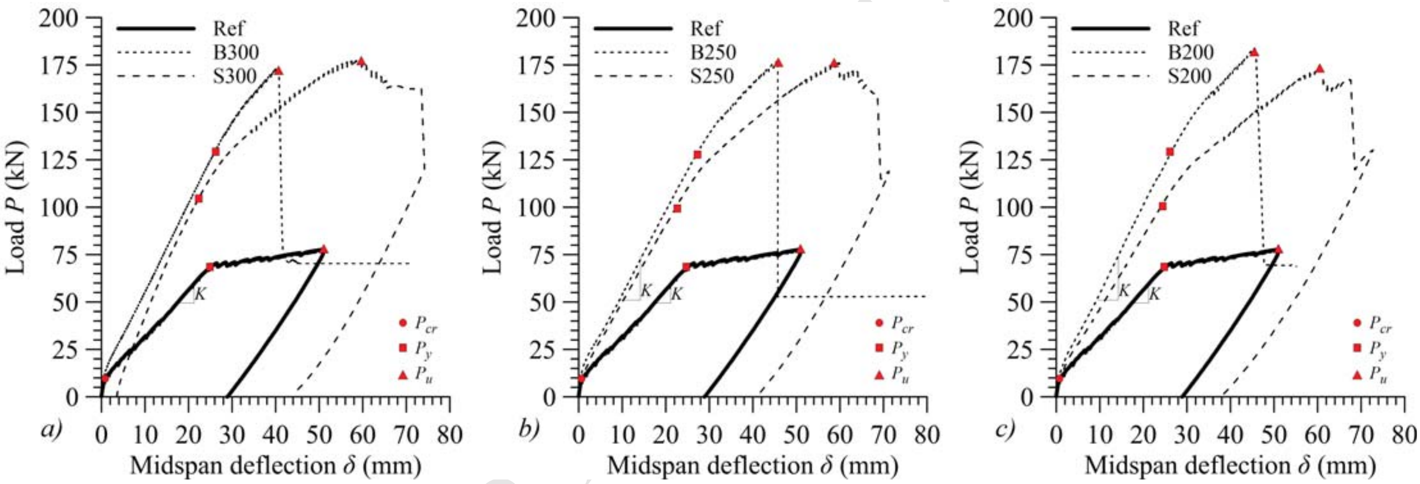

200
175
150
125
100
75
50
25
0
Load P (kN)
Ref
B300
S300
B250
S250
B200
S200
K
P_{cr}
P_y
P_u
a)
b)
c)
0 10 20 30 40 50 60 70 80
Midspan deflection δ (mm)

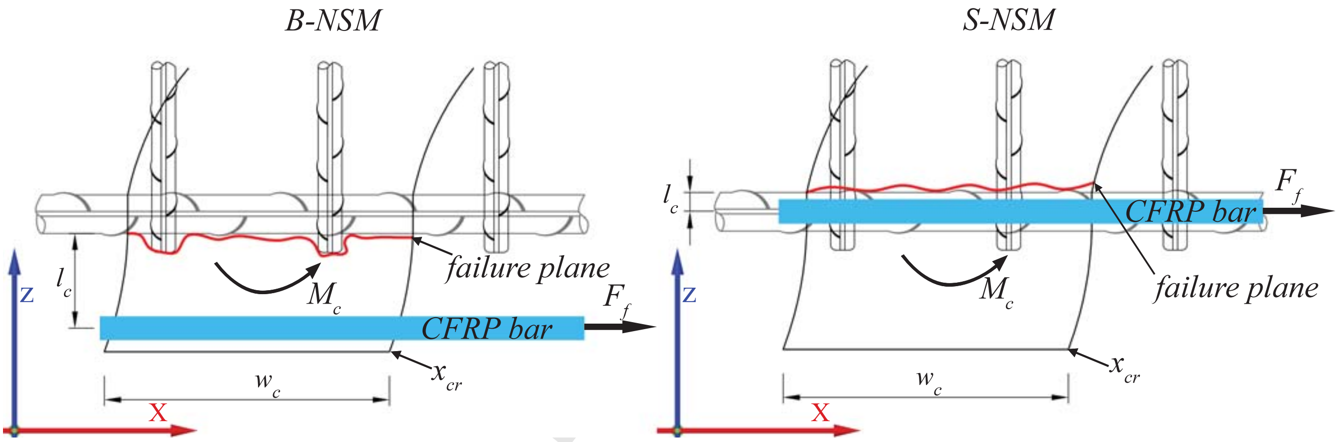
B-NSM
failure plane
l_c
M_c
F_f
CFRP bar
x_{cr}
w_c
Z
X
S-NSM
l_c
F_f
CFRP bar
failure plane
M_c
x_{cr}
w_c
Z
X

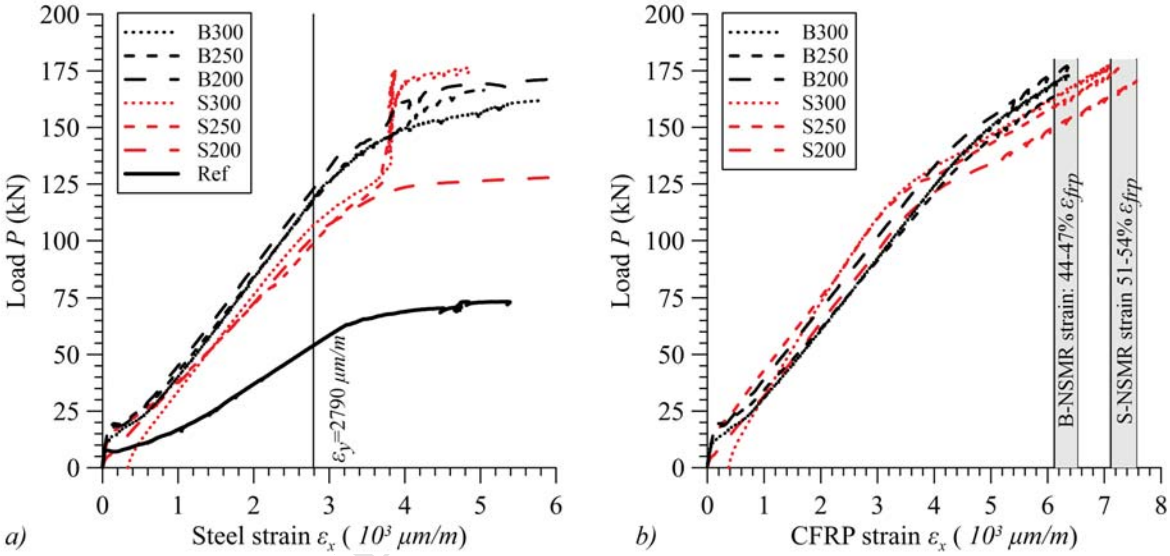
B300
B250
B200
S300
S250
S200
Ref
Load P (kN)
εy=2790 μm/m
a)
Steel strain εx (10³ μm/m)
B-NSMR strain: 44-47% εfrp
S-NSMR strain 51-54% εfrp
b)
CFRP strain εx (10³ μm/m)